ACTA METALLURGICA SLOVACA
2024, VOL. 30, NO. 3, 133-136

RESEARCH PAPER

# SYNTHESIS OF AN ALUMINUM ALLOY RICH IN IRON AND SILICON BY SURFACING WITH A CONSUMABLE ELECTRODE

*Violetta Andreyachshenko[1,*], Igor Bartenev[2], Yelena Malashkevichute-Brillant[3]*

[1] Abylkas Saginov Karaganda Technical University, 100027, Karaganda, Kazakhstan, Vi-ta.z@mail.ru,
[2] Abylkas Saginov Karaganda Technical University, 100027, Karaganda, Kazakhstan, igor_svar@mail.ru,
[3] Abylkas Saginov Karaganda Technical University, 100027, Karaganda, Kazakhstan, elenei66@mail.ru

*Corresponding author: Vi-ta.z@mail.ru, tel.: 87013962994, Abylkas Saginov Karaganda Technical University, 100027, Karaganda, Kazakhstan

Received: 02.08.2024
Accepted: 24.08.2024

## ABSTRACT

Developing lightweight, high-strength materials is an important technological problem of the present decade. However, alloying with expensive elements is mainly used to increase the strength of structural materials. In contrast, aluminum alloys with a specific ratio of silicon and iron show very high mechanical properties. This work aims to develop a technology for synthesizing an aluminium-based alloy with a high content of iron and silicon, consisting mainly of intermetallic phases and having high strength and hardness. The additive technology method of surfacing with a consumable electrode produced the alloy. The ratio of the initial components, meticulously determined, led to the precise chemical composition of the alloy. As a result of the synthesis, an ingot with a uniform microstructure and insignificant porosity, a testament to the careful process, was obtained. At room temperature, the alloy has a phase composition of 42.6% β-phase, 43.4% θ-phase and 13.5% FCC-phase. Phases β and θ are large particles between which the FCC aluminum phase is located. The hardness of the intermetallic β/θ is 450.8±5 HV1, FCC aluminum has a hardness of 92.5 HV1. This research has the potential to inspire further developments in materials science and engineering.

**Keywords:** Al-Fe-Si, synthesis, additive technology, microstructure, hardness

## INTRODUCTION

In recent years, researchers worldwide are increasingly faced with improving aluminium alloys' properties [1-3]. In addition, various metal-ceramic materials, high-entropy materials and alloys are being developed [4-6]. A significant problem is treating aluminium scrap since, during recycling, aluminium is inevitably contaminated with impurities, primarily iron [7-9]. In recent decades, a wide range of studies has been aimed at synthesising and studying iron and silicon-enriched aluminium alloys; however, when mentioning a high iron content, they are, as a rule, talking about the content of no more than 5% [10-12].

At the same time, very few works deal with aluminium alloys with an iron content of more than 10 and 20%. This is primarily due to the complicated process of obtaining such a group of alloys [13]. The differences in the melting point mainly cause the difficulties. For example, aluminium has a melting point of 660 °C, silicon 1414 °C, and iron 1539 °C. In addition, differences in the type of crystal lattice and atomic sizes preclude producing solid solutions with a significant amount of dissolved components. Success in producing such complex alloys can be achieved using powder metallurgy and additive technologies; the latter seems more promising. The use of the principle of the material layer-by-layer addition significantly expands the possibilities of producing complex, poorly fused materials using additive methods. In contrast, using an electric arc as a factor initiating synthesis provides temperatures up to 3000-5000 °C and higher. Traditionally, the surfacing method is used to restore worn elements of machine parts or structural components, but the possibility of using the technique for synthesizing new materials is increasingly used.

It is known that alloys of the Al-Fe-Si system with a low content of alloying elements are well subject to plastic deformation, capable of grain refinement to an ultra-fine-grained state and maintain fairly high ductility [14-16].

However, as the alloying components' content increases, the alloy's ductility gradually decreases. When a certain percentage is reached, intermetallic compounds can predominantly represent the phase composition [17-20]. It is traditionally believed that the β-phase has a needle-like structure, and the θ-phase is present in the form of plates or needles [21-24]. However, the authors of [25] found that the αc-AlFeSi phase can develop on top of the β-AlFeSi phase layer, which leads to the absence of the traditional morphology of the β-AlFeSi phase.

## MATERIAL AND METHODS

The Al-Fe-Si system alloy was synthesized using the additive method, by surfacing with a horizontal consumable electrode. To obtain the specified composition, we used commercial aluminum alloy AD31N (composition aluminum 90%, silicon 2%, iron 0.5%) in sheets 2 mm thick, commercial steel grade St3 (composition iron 95%, silicon, manganese) in sheets 2 mm thick mm and 5 mm and silicon fraction -500 microns (composition silicon 99%, aluminum 1%. A steel sheet 2 mm thick was

cut into blanks measuring 15x20x2 mm and used as electrodes. Aluminum sheet was cut into blanks measuring 100x30x2 mm. Silicon was crushed in a vibrating machine to a fraction of -70 microns with pre-drying in a SNOLL 67/350 chamber oven at a temperature of 115 °C within 20 minutes, then applied to aluminum plates at the rate of 2.5 grams of silicon per 15 grams (1 plate) of aluminum using a wet method followed by drying at room temperature for at least 12 hours. To obtain the Al60Fe30Si10 composition, a package was formed, consisting of 4 aluminum plates coated with silicon and a steel plate in the form of an electrode. The prepared package was laid horizontally on a steel base plate 5 mm thick. A steel plate measuring 150x20x2 mm is installed on top of the package through a layer of welding flux as an electrode. Then, cables were connected from the welding power source to the electrode and base. The package and the electrode were covered on top with a 20 mm thick layer of AN-348 welding flux (**Fig. 1**). For the synthesis, and a power source was used for melting the alloy components: a VDM-1202 welding rectifier with an RB-301 ballast rheostat. A stationary filter-ventilation welding table SS-1200/SP was used to carry out the experiments.

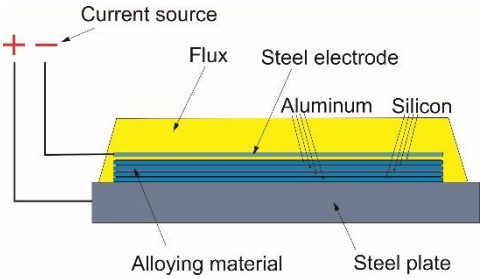


**Fig. 1** Scheme of the synthesis process

After turning on the welding source and exciting the electric arc, the steel electrode and the package of aluminum plates are melted. The welding current is 290 A. The melting time of the electrode and the package is 10 seconds on average. The melting process takes place autonomously, without any external regulation. After the package and electrode have completely melted, the power source is turned off, and the resulting alloy lying on the steel base under the layer of molten flux is cooled. After removing the slag crust, an alloy ingot was obtained, which was cut using a cutting machine with cooling Unitom-2 into templates for metallographic analysis, assessment of the hardness level and determination of the chemical composition. Microsections for metallographic analysis were prepared using standard methods on a Labotom-5 grinding machine using lubricants and studied on an Altami MET 5T optical microscope. The hardness was measured on plane-parallel samples using the Vickers method with a Wilson VN1150 hardness tester.

The chemical composition of the synthesized alloy was monitored using an X-ray fluorescence analyzer Vanta Element-S from Olympus with the option of detecting light elements. For a better interpretation of the results obtained, a phase composition diagram was constructed to assess the mass fraction of the formed phases in the temperature range from 1500 °C to room temperature. To construct the phase diagram, the ThermoCalc software version 2024a, the TCAL8 database: Al-Allous v8.2 was used. During construction, the composition was specified in weight %, considering the impurities in steel, aluminum and silicon.

## RESULTS AND DISCUSSION

### The synthesizing process

The process of alloy synthesis is accompanied by the melting of alloy components by an electric arc, as well as flux, which effectively protects the alloy from oxidation directly during the synthesizing process. The layer of molten flux also prevents the active transition of alloy components to waste and evaporation, because the arc temperature averages 5000 °C. After complete melting of the steel electrode and the package of aluminum plates with silicon powder, completion of the arc combustion and complete cooling, a dense glassy porous slag crust is formed that is removed after cooling. Fusion of the resulting alloy with the steel substrate and penetration of steel into the alloy does not occur. As a result of the synthesizing process, an ellipse-like alloy ingot with average dimensions of 30.9x12.5x100 mm is formed (**Fig. 2**). When synthesizing the initial package from wafers and powdered silicon, a slight melting of the side faces is observed with-out significant spreading of the metal. The side ends acquire a rounded shape, while the initial components of the prepared package interact with each other to produce a homogeneous material. Heavier iron atoms sink, forming intermetallic compounds with aluminum and silicon. The layer-by-layer arrangement of silicon reduces segregation, thereby ensuring the chemical composition uniformity throughout the entire cross-section of the ingot. The advantage of this arrangement and introduction of initial components into the molten bath is the uniform distribution of iron in the molten aluminium bath that ensures uniformity of the chemical composition of the ingot without additional mixing.

It is worth noting that high synthesis temperatures lead to the intense destruction of the oxide film on aluminium and, consequently, abundant gas formation. Due to the intensity of the process, gases do not have time to escape from the molten metal bath entirely. This leads to some pore formation, which also coincides with the results of [26]. Moreover, the gas permeability of the molten flux (slag) depends on the welding flux's particle size distribution and its production method. In additional experiments, surfacing was carried out using a pumice-like ceramic flux with better gas permeability than the glassy fused flux AN-348.

### Chemical and phase composition

Previous studies of the three-component Al-Fe-Si system showed that the alloy with the composition Al60Fe30Si10 in wt. % has a preferable composition among the alloys of this system, which is rich in iron and silicon [27]. At the same time, the charge materials used are not pure, so additional chemical elements inevitably end up in the finished alloy during synthesis. Besides, the flux, in addition to protecting the metal bath from oxidation, also comes into contact with the molten metal, making certain adjustments to the basic (planned) chemical composition. The chemical composition of the resulting alloy is shown in **Table 1**.


**Fig. 2** Appearance of the synthesized material

The resulting composition has a reduced content of iron and especially silicon. This is explained by the transition of some of

these elements into the slag crust, while manganese, being reduced from the oxide, penetrates into the metal from the flux.

**Table 2** Chemical composition of the synthesized alloy

| Name | Chemical composition, wt. % | | | | | | | | |
|---|---|---|---|---|---|---|---|---|---|
| | Al | Fe | Si | Mn | P | S | Ni | Sc | Cu |
| Alloy Al60Fe30Si 10 | 66.40 | 29.54 | 3.72 | 0.183 | 0.05 | 0.03 | 0.024 | 0.023 | 0.017 |

To clarify the possible phase composition and based on the actual chemical composition, a phase diagram was constructed, according to which at room temperature the phase composition of the alloy includes 42.6% β-phase, 43.4% θ-phase and 13.5% FCC phase. Manganese can partially replace iron, and the θ-phase, like the FCC phase, dissolves a small amount of impurities but mainly impurity elements form compounds with aluminum: Al1P1, Al2S3, Al3Ni, Al7Cu2Fe and Al3Sc. The volume fraction of these compounds does not exceed 0.15% and they are probably presented in the form of disper-soids. The refined phase composition makes it possible to interpret the results of metallographic analysis more accurately. However, it is worth considering that the calculation of the phase diagram is carried out for equilibrium conditions, while during synthesis the conditions are not equilibrium; there is directed heat removal through the base plate and through the slag crust, which can lead to the appearance of residual phases in the final phase composition.

**Metallographic analysis and hardness**

The analysis has been carried out on samples as received, i.e. immediately after synthesis. When examining a sample, one can consider a continuous series of intermetallic compounds formed after crystallization. Throughout the entire area of the sample there are intermetallic compounds, elongated, strictly oriented in one direction over a large extent. The morphology of the location of the phase components indicates the presence of directed heat removal normal to the plane of the synthesized material. First of all, heat is removed through the base plate, and simultaneously but to a lesser extent, through the slag crust, which is directly cooled through contact with the surrounding atmosphere. The lateral heat removal is reduced due to the unmelted flux located at the edges of the synthesized material. In general, a slight gradient of the microstructure, consisting of two main components, is observed on the microsection. These are intermetallic compounds (gray zones in photograph) occupying about 70% of the studied microsection area in the upper region of the sample, and about 90% closer to the lower zone in contact with the base plate and lighter areas. The gray region consists entirely of β/θ intermetallic compounds. It can be seen in optical micrographs (Fig. 3b and 3c) that obtained at high magnifications, the light areas represent a complex consisting of an FCC solid solution, a mechanical mixture-eutectic in the form of a solid solution based on aluminum and silicon and dispersed intermetallic inclusions of needle-shaped and skeletal forms. Moreover, this type of phase arrangement is typical for light areas over 100 μm thick. A supersaturated solid solution is observed in thinner layers of light microsection components, with β-phase particles located in some areas. The absence of a clearly defined characteristic θ-phase is due to the peculiarities of the formation of intermetallic phases and the multi-stage formation of the structure during cooling. Dark rounded areas up to 10 μm in size are observed exclusively in the light zones of the microsection under study. They are probably elements of the oxide film covering the aluminum plates. The sample contains pores, presumably associated with the high speed of the synthesizing process.

The β-phase morphology is related to the selected alloy composition. During crystal-lization, crystals of two-component phases are first of all formed from the liquid: the θ- phase and aluminum compounds with impurities. Particles of the θ-phase serve as cen-ters of crystallization of the α-phase, which then transforms into the β-phase. This nature of phase formation leads to the fact that the particles of the θ-phase are the nuclei of larger secondary particles of the β-phase that develop until the surrounding liquid is depleted of both silicon and iron. In contrast, the remaining liquid crystallizes according to the crystalliza-tion scheme of aluminum alloys enriched with iron and silicon atoms, by forming a eu-tectic. The phenomenon when one of the phases serves as the nucleus of particles of an-other phase has already been encountered and described in the scientific literature [28]. The reduced number of particles of β/θ-phases in the upper part of the ingot is explained by the reaction of iron atoms with the molten flux and the formation of iron-containing complex compounds, which in turn leads to the difficulty of separating the slag crust, and on the other hand, to a composition gradient along the height of the ingot.

Among all the phase components considered, the β/θ-phases have the highest hard-ness value that reaches 450.8±5 HV1. When measuring phases with smaller sizes, when in the zone of indenter influence, the microhardness is 360±6 HV1, and that of the solid solution region, despite the dispersed intermetallic particles located there, is 92.5 HV1. It is worth noting that the regions of β/θ-phases and solid solution have a spatial formation pattern, which is confirmed by the presence of thickness contrast in micrographs and the destruction of the indenter imprint at small layer thicknesses with the recording of inter-mediate hardness values. No hardness values were found within the β/θ-gradient phase regions themselves.

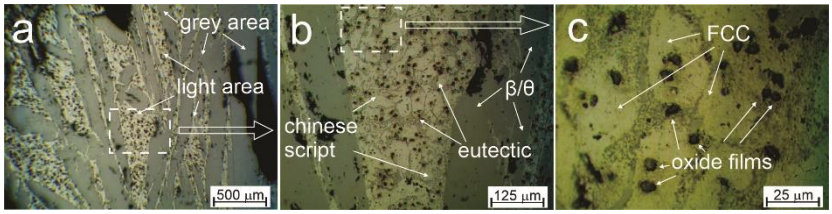


**Fig. 3** Optical photography of the microstructure of the synthesized alloy at various magnifications: (a) x100; (b) x400; (c) x1000

**CONCLUSION**

The proposed new synthesizing method effectively combines dissimilar elements such as aluminum, silicon, and iron to produce a compact ingot.

The method has been proposed for arranging the synthesized components to ensure the production of an alloy with a homogeneous microstructure without additional mixing.

The alloy was obtained, 86.5% consisting of an intermetallic compound with the hardness of 450.8 ± 5 HV1, alternating with FCC aluminum with the hardness of 92.5 HV1.

**Acknowledgements:** This research was funded by the Science Committee of the Ministry of Science and Higher Education of the Republic of Kazakhstan (Grant No. AP19675471).

**REFERENCES**

1. P. Mikolajczak: Materials, 16 (9), 2023, 3304. https://doi.org/10.3390/ma16093304.
2. V. Andreyachshenko: Materials Letters, 254, 2019, 433–435. https://doi.org/10.1016/j.matlet.2019.07.127.
3. C. G. McKamey, J. H. DeVan, P. F. Tortorelli, V. K. Sikka: Journal Materials Research, 6, 2011, 6, 1779–1805. https://doi.org/10.1557/JMR.1991.1779.
4. N. Kota, M. S. Charan, T. Laha, S. Roy: Ceramics International, 48(2), 2022, 1451-1483. https://doi.org/10.1016/j.ceramint.2021.09.232.
5. M. Rogala, W. Tuchowski, D. Czarnecka-Komorowska, K. Gawdzińska: Advances in Science and Technology Research Journal, 16(4), 2022, 287–297. https://doi.org/10.12913/22998624/153028.
6. M. Asadikiya, S. Yang, Y. Zhang, C. Lemay, D. Apelian, Y. Zhong: Journal of Materials Science, 56, 2021, 12093-12110. https://doi.org/10.1007/s10853-021-06042-6.
7. D. Song, Y. Jia, Q. Li, Y. Zhao, W. Zhang, Materials, 15(4), 2022, 1618. https://doi.org/10.3390/ma15041618.
8. N. Pang, Z. Shi, C. Wang, N. Li, Y. Lin: Materials, 14(4), 2021, 768. https://doi.org/10.3390/ma14040768.
9. E. de Rosso, C. A. dos Santos, A. Garcia: Advanced Engineering Materials, 24(8), 2022, 2001552. https://doi.org/10.1002/adem.202001552.
10. W. C. Yang, G. A. O. Feng, S. X. Ji: Transactions of Nonferrous Metals Society of China, 25(5), 2015, 1704-1714. https://doi.org/10.1016/S1003-6326(15)63776-1.
11. Z. Que, C. L. Mendis: Intermetallics, 127, 2020, 106960. https://doi.org/10.1016/j.intermet.2020.106960.
12. M. V. Canté, T. S. Lima, C. Brito, A. Garcia, N. Cheung, J. E. Spinelli: Journal of Sustainable Metallurgy, 4, 2018, 412-426. https://doi.org/10.1007/s40831-018-0188-y.
13. R. Kakitani, A. V. Rodrigues, C. Silva, A. Garcia, N. Cheung: Journal of Alloys and Metallurgical Systems, 1, 2023, 100005. https://doi.org/10.1016/j.jalmes.2023.100005.
14. V. A. Andreyachshenko, Y. Isheva, A. Mazhit, D.Imangazinova: Materials & Technologies/Materiali in Tehnologije, 53(6), 2019, 805-810. https://doi.org/10.17222/mit.2018.250.
15. J. Bidulská, T. Kvackaj, I. Pokorny, R. Bidulsky, M.A. Grande: Archives of Metallurgy and Materials, 58(2), 2013, 371-375. https://doi.org/10.2478/amm-2013-0002.
16. V.A. Andreyachshenko: Kovove Materialy-Metallic Materials, 60 (2), 2022, 79-87. https://doi.org/10.31577/km.2022.2.79.
17. Z. Que, Y. Wang, C. L. Mendis, C. Fang, J. Xia, X. Zhou; Z. Fan: Metals, 12(10), 2022, 1677. https://doi.org/10.3390/met12101677.
18. Z. Que, C. Fang, C. L. Mendis, Y. Wang, Z. Fan: Journal of Alloys and Compounds, 932, 2023, 167587. https://doi.org/10.1016/j.jallcom.2022.167587.
19. V. Andreyachshenko, A. Toleuova: Kompleksnoe Ispolzovanie Mineralnogo Syra= Complex use of mineral resources, 332(1), 2025, 98-107. https://doi.org/10.31643/2025/6445.09.
20. A. B. Naizabekov, V. A. Andreyachshenko: Metallurgist, 57 (1-2), 2013, 159–163. https://doi.org/10.1007/s11015-013-9706-0.
21. Zhang, D. Wang, X. Li, H. Zhang, H. Nagaumi: Intermetallics, 131, 2021, 107103. https://doi.org/10.1016/j.intermet.2021.107103.
22. P. Orozco-González, M. Castro-Román, R. Muñiz-Valdez, S. Luna-Álvarez, F. Equihua-Guillén, A. Hernández-Rodríguez, V. H. Baltazar-Hernández, F. Alvarado-Hernández: Materials Letters, 180, 2016, 277-279. https://doi.org/10.1016/j.matlet.2016.05.139.
23. H. Jiang, Y.C. Liu, C. Wei, Y. H. Zhang, Z. M. Gao: Journal of Alloys and Compounds, 466(1–2), 2008, 92-97. https://doi.org/10.1016/j.jallcom.2007.11.019.
24. J. M. Yu, N. Wanderka, A. Rack, R. Daudin, E. Boller, H. Markötter, A. Manzoni, F. Vogel, T. Arlt, I. Manke, J. Banhart: Journal of Alloys and Compounds, 766, 2018, 818-827. https://doi.org/10.1016/j.jallcom.2018.06.372.
25. T. Smith, K. O'Reilly, S. Kumar, I. Stone: Metallurgical and Materials Transactions A, 44, 2013, 4866-4871. https://doi.org/10.1007/s11661-013-1934-1.
26. G. Casalino, P. Leo, M. Mortello, P. Perulli, A. Varone: 7(8), Metals, 2017, 282. https://doi.org/10.3390/met7080282.
27. V. A. Andreyachshenko, M. K. Ibatov: Metallurgical Research & Technology, 121(3), 2024, 315. https://doi.org/10.1051/metal/2024035.
28. H. Becker, T. Bergh, P. E. Vullum, A. Leineweber, Y. Li: Materialia, 5, 2019, 100198. https://doi.org/10.1016/j.mtla.2018.100198.